ACS APPLIED ENERGY MATERIALS

www.acsaem.org

Article

Solvent-Dependent Charge Transfer Dynamics under Indoor Light in Efficient and Stable Copper-Mediated DSSCs

Fátima Santos,* Dzmitry Ivanou, and Adélio Mendes

Cite This: *ACS Appl. Energy Mater.* 2026, 9, 8868−8878

Read Online

ACCESS | Metrics & More | Article Recommendations | Supporting Information

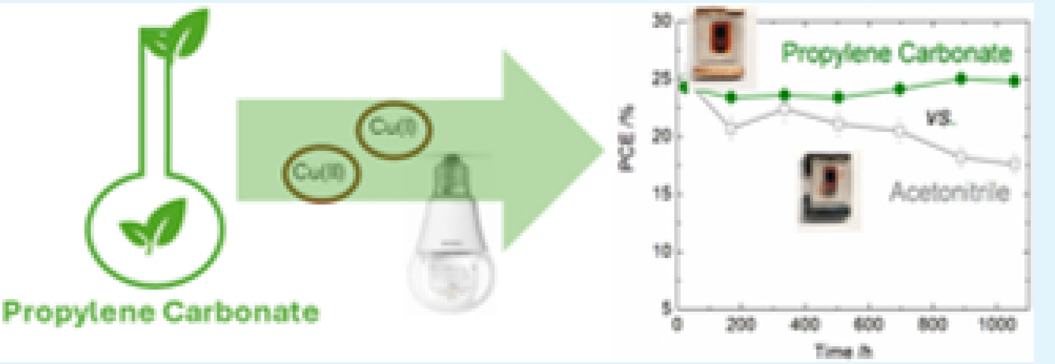

ABSTRACT: Indoor photovoltaics (iPVs) are emerging as a sustainable and reliable power source to address the growing energy demands caused by the rapid expansion of the Internet of Things ecosystem. Combining high photovoltaic performance under indoor light with low-cost, simple production, and pleasant aesthetics, copper-mediated monolithic dye-sensitized solar cells (DSSCs) are a strong candidate for iPVs. Efforts have been made to replace expensive and scarce materials used in the preparation of conventional DSSCs with more abundant and sustainable materials. However, DSSCs still employ materials with considerable toxicity, namely, the nitrile-based solvents in the electrolyte solutions. This work considers for the first time propylene carbonate (PC), γ-butyrolactone (GBL), and N-methyl-2-pyrrolidone (NMP) as candidates for the electrolyte solvent in indoor DSSCs. Among them, PC-DSSCs display power conversion efficiencies (PCEs) competitive with those of 3-methoxypropionitrile-based devices under light intensities between 300 and 1000 lx; both are able to maintain PCEs above 25%. Time-resolved photoluminescence measurements reveal a clear electrolyte donor number-dependent modulation of interfacial electron injection and radiative relaxation dynamics from excited states, which correlates with device performance under weak indoor light. Among other solvents, this study demonstrates PC as a safe, sustainable electrolyte solvent for efficient and stable indoor DSSCs.

KEYWORDS: *dye-sensitized solar cells, monolithic, indoor photovoltaics, low-volatile solvents, electrolyte*

1. INTRODUCTION

In the early 1990s, dye-sensitized solar cells (DSSCs) arose from the need to develop cost-effective alternatives to silicon solar panels. Their unique properties, which combine low-cost and non-toxic materials, a semi-transparent and colorful appearance, and good efficiency under diffuse light, made them a strong candidate for building-integrated photovoltaics (BIPVs).[1] Later, with the exponential growth of Internet of Things (IoT) devices, DSSCs emerged as front-runners in indoor photovoltaics (iPVs), due to their aesthetic appeal and the spectral matching between indoor light sources and dye absorption, enabling power conversion efficiencies (PCEs) exceeding 30% under indoor illumination.[1,2]

To date, the highest energy-performing DSSCs, regardless of light intensity, utilize a copper redox mediator with nitrile-based solvents.[3−5] An organic solvent must fulfill several requirements to be suitable as an electrolyte solvent in DSSCs: it should allow for high solubility of redox mediators and salts, thereby promoting a high ionic mobility; exhibit low light absorption; be inert regarding the dye molecules attached to the TiO_2 surface; have a low cost; and be non-toxic.[6,7] The most critical parameters for selecting the electrolyte solvent are its viscosity, boiling point, dielectric constant, and donor number. A solvent with low viscosity will facilitate the ionic mobility, and a high boiling point will cause slower evaporation, contributing to minor leakage

Received: April 23, 2026
Revised: June 12, 2026
Accepted: June 15, 2026
Published: June 30, 2026

https://doi.org/10.1021/acsaem.6c01356
ACS Appl. Energy Mater. 2026, 9, 8868−8878

through the device's sealed perimeter. The ability to dissociate salts is enhanced with a solvent with a higher dielectric constant. At the same time, the tendency to donate an electron pair can be enhanced by selecting a solvent with a higher donor number. Moreover, a high donor number causes an upshift of the TiO_2 conduction band, increasing the open-circuit potential difference (V_{OP}) of the devices, though also reducing the short-circuit current (J_{SC}).[6] Due to its low viscosity, excellent chemical stability, and ability to dissolve salts and organic molecules, acetonitrile (ACN) is still the preferred electrolyte solvent for highly efficient DSSCs. Though its high volatility may compromise the long-term performance of these devices.[6,7]

Under AM1.5G, several alternative solvents have been reported for DSSCs, including 3-methoxypropionitrile (MPN), dimethylformamide (DMF), propylene carbonate (PC), γ-butyrolactone (GBL), N-methyl-2-pyrrolidone (NMP), and acetylacetone.[8−13] Although these devices displayed lower PCE than the ACN-based DSSCs, all of them reported improvements in their long-term performance.

The irradiance of ambient light is two to three orders of magnitude lower than the solar irradiance.[14] Therefore, the generated photocurrent is typically two to three orders of magnitude lower, depending on indoor irradiance, spectral mismatch, and device characteristics, among others.[14] Hence, the concentration of redox species in the electrolyte solutions has been adjusted to balance the ionic conductivity and the recombination rate.[4,15−19] However, less attention has been paid to the electrolyte solvent: only a few works have considered alternatives to the ACN solvent, most of them using nitrile-based solvents.[4,5,14,20,21] To date, the highest reported PCE for indoor DSSCs, 38.0% (1000 lx), was achieved with a copper-based electrolyte containing 3-methoxypropionitrile.[4] Recently, Speranza et al.[22] reported γ-valerolactone as a sustainable and low-toxic electrolyte solvent for iodide-mediated DSSCs operating indoors.

This study investigates the impact of different electrolyte solvents (MPN, PC, GBL, and NMP) on the performance and stability of copper-mediated monolithic DSSCs (M-DSSCs) under ambient light, and compares the results with those obtained with the corresponding ACN-based devices. The obtained photovoltaic performance were correlated with the physicochemical properties of the solvent used (Table 1), such as polarity, viscosity, and donor number, and the redox activity of the electrolyte, as well as photogenerated carrier lifetimes and diffusivity, interfacial charge-transfer dynamics, and lifetimes of the excited states. Except for the DSSCs using NMP as the electrolyte solvent, the devices using the other organic solvents showed similar performance or even outperformed those employing an ACN-based electrolyte. Furthermore, the devices using MPN and PC showed minute fluctuations in their PCE with the light intensity, due to small potential difference losses and a decrease in fill factor: 27.6−28.5% (300−1000 lx) for MPN-DSSCs, and 26.0−27.1% (300−1000 lx) for PC-DSSCs. In comparison with MPN, PC has the advantage of being considered a green solvent with low toxicity. Thus, this work presents PC as a sustainable and safe alternative to the nitrile-based solvents for copper-mediated indoor DSSCs.

2. EXPERIMENTAL SECTION

2.1. Reagents and Materials

The FTO-coated glass substrates (7 $\Omega \cdot sq^{-1}$) and the TiO_2 pastes (18NR-T and WER2-O) were acquired from GreatCell Solar. 2-propanol (anhydrous, 99.5%), titanium diisopropoxide bis(acetylacetonate) (75 wt% in 2-propanol), acetylacetone (>99.5%), α-terpineol (>96.0%), *N*-methylbenzimidazole (NMB, 99.0%), ACN (anhydrous, 99.8%), MPN (≥98.0%) and PC (≥99.7%) were purchased from Sigma-Aldrich. Graphite/carbon-black paste (Elcocarb B/SP), chenodeoxycholic acid (CDCA), and thermoplastic sealant (Surlyn, 60 μm) were ordered from Solaronix. $[Cu(tmby)_2(TFSI)_{2/1}]^{2+/+}$ complexes, Y123 and XY1b sensitizers were bought from Dyenamo. Titanium tetrachloride (99.9%), *t*-butanol (99.5%), and lithium bis(trifluoromethanesulfonimide) (LiTFSI, 98.0%) were received from Acros Organics. From Alfa Aesar and Fisher Scientific, GBL (≥99.0%) and NMP (99.0%) were obtained, respectively. Absolute ethanol (100%) was acquired from Merck; tetrahydrofuran (THF, ≥99.9%) was ordered from Honeywell.

Table 1. Molecular Structure and Physical Properties of Solvents Used in the Preparation of Electrolyte Solutions of DSSCs[6a]

	Molecular structure	Viscosity /cP	Melting point /°C	Boiling point /°C	Dielectric constant	Donor number (DN) /kJ mol^{-1}
ACN		0.33 (30 °C)	-44.0	81.6	37.5 (20 °C)	59.0
MPN		1.10	-63.0	164.0	36.0	67.4
NMP		1.65	-24.0	203.0	32.2	114.3
PC		2.50	-49.0	241.0	64.0	63.2
GBL		1.70	-44.0	204.0	42.0	75.4

[a]All data at 1 atm and 25 °C except the ones specified.

2.2. Fabrication of M-DSSCs

Since the DSSCs were prepared in a monolithic configuration (Figure 1), mechanical scribing was performed on the FTO-coated glass substrates to separate both electrodes. Then, the FTO-coated glasses were cleaned in an ethanolic KOH solution and water, and treated with air plasma for 10 min. A TiO_2 blocking layer was deposited by spray pyrolysis at 450 °C from a solution composed of 2-propanol, titanium diisopropoxide bis(acetylacetonate), and acetylacetone. An 18NR-T titania paste diluted in α-terpineol (paste:α-terpineol = 2:1, by mass) was applied by screen-printing to prepare the mesoporous TiO_2 layer; after sintering at 500 °C for 1 h, a 4.5 ± 0.5 μm-thick TiO_2 layer was obtained. At this moment, a 20 mM $TiCl_4$ solution was used in the post-treatment of the mesoporous TiO_2 layer (70 °C, 30 min), followed by annealing at 500 °C for 1 h. Then, a TiO_2-rutile WER2-O paste diluted in α-terpineol (paste:α-terpineol = 2:1, by mass) was deposited by screen-printing to form a TiO_2 insulating/spacer layer; a 4.5 ± 0.5 μm-thick TiO_2 spacer layer was obtained after sintering for 1 h at 500 °C. Immediately after, a paste composed of a mixture of carbon-black nanoparticles and 20 μm graphite (Elcocarb B/SP paste) was applied by doctor-blading to prepare the counter-electrode layer; a 23 ± 3 μm-thick carbon-based layer was attained after annealing for 45 min at 420 °C. The devices were then immersed for 48 ± 2 h in a dye solution with an equal volume of 0.2 mM Y123 dye in ACN:*t*-butanol (1:1 volume ratio), and 0.2 mM XY1b dye + 5.0 mM CDCA in THF:ethanol (1:4 volume ratio) – chemical structures of Y123 and XY1b dyes presented in Figure S1. After this period, the devices were cleaned with ACN, dried under a N_2 flow, and assembled in a sandwich structure

https://doi.org/10.1021/acsaem.6c01356
ACS Appl. Energy Mater. 2026, 9, 8868−8878

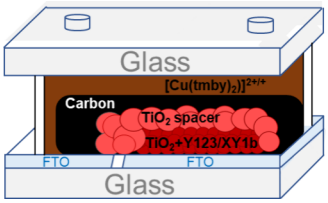

Figure 1. M-DSSC architecture of the devices used in the present work.

using an ordinary top glass with pre-drilled holes and a piece of Surlyn; both glasses were bonded together using a manual hot press. The electrolyte solution was injected into the cell through the holes in the ordinary glass; this formulation was composed of 0.1 M Cu(I)(tmby)$_2$TFSI, 0.04 M Cu(II)(tmby)$_2$(TFSI)$_2$, 0.1 M LiTFSI, and 0.6 M NMB in different solvents (ACN, MPN, NMP, PC, or GBL) – chemical structures of the copper complexes presented in Figure S1. The infiltration of the electrolyte solution into TiO_2 pores was enhanced by applying a vacuum right after electrolyte injection. A thermoplastic film and a lamella glass were used to close the holes.

2.3. Fabrication of Symmetrical Half Cells

The symmetrical half cells (active area of 0.25 cm^2) were prepared by depositing a layer of Elcocarb B/SP paste on FTO-coated glass substrates and annealing for 45 min at 420 °C, resulting in a 23 ± 3 μm-thick layer. Two 60 μm-thick thermoplastic films were then used to assemble two identical FTO-supported electrodes. Two holes were previously drilled in one of the FTO-supported electrodes; the electrolyte was inserted into the half-cells through these holes. Finally, the holes were closed using a piece of thermoplastic film and a lamella glass.

2.4. Characterization

The symmetrical half cells were characterized by cyclic voltammetry and electrochemical impedance spectroscopy at 0 V, scan rate of 5 mV s^{-1}, and in dark conditions using an Autolab electrochemical station (PGSTAT 302 N, Metrohm). The impedance data were analyzed using ZView software; the series resistance (R_S), the charge-transfer resistance at the electrolyte/electrode interface (R_E), the finite-length Warburg element (W_S), given by the modulus of the Warburg impedance, and the constant phase element for the electrolyte/electrode interface (CPE) were determined by fitting the impedance response with the equivalent circuit presented in Figure 2.

The J–V characteristics of the M-DSSCs were recorded using a Zennium (Zahner) electrochemical station. For measurements under simulated solar light (AM1.5G, 100 mW·cm^{-2}) was used a Class ABA Led Solar Simulator (MiniSol LSH-7320, Newport), and the photoanode was masked with a 0.071 cm^2 aperture mask.

The light source for measurements under artificial light was an LED lamp (Osram, 60 W, 2700 K, with a spectral onset at 95% cumulative irradiance at ca. 676 nm[23]), whose emission spectrum is presented in Figure S2. Their emission spectra were obtained using a Getspec 2048 spectrometer. The J–V characteristics under artificial illumination were recorded at three different light intensities: 300 lx (0.08 W m^{-2}), 600 lx (1.66 W m^{-2}), and 1000 lx (2.75 W m^{-2}), with the photoanode masked using a 0.126 cm^2 aperture mask. The illuminance power of the LED lamp (in Lux and μW cm^{-2}) was measured using a radiometer (Delta Ohm HD 2102.2). The PV metrics of three identical devices were used to determine the average PV metrics for each tested condition. The influence of the angular-response errors on the PCE of these devices was evaluated as described in ref 24; since the PCE variation was less than 5%, the accuracy of the reported PCEs was confirmed (Table S1). The set-up for indoor PV characterization is presented in Figure S3.

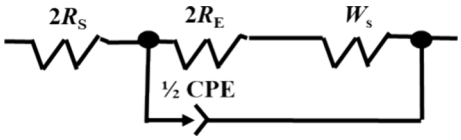

Figure 2. Electrical equivalent circuit used to fit the impedance response of symmetrical half cells.

EIS data of M-DSSCs were collected and analyzed according to the procedure outlined for symmetrical half-cells. The differences rely on the applied voltage (0 V in half cells *vs.* open-circuit voltage in M-DSSCs) and on the equivalent circuit (Figure 2 in half cells *vs.* transmission line model by Bisquert in M-DSSCs).[25]

The transmittance of TiO_2 + dye photoanodes immersed in the different electrolyte solvents for 24 h was measured using a UV-3600i Plus UV-Vis-NIR spectrometer (Shimadzu) with an ISR-1503 integrating sphere.

The lifetimes of the photoexcited states were monitored by Time-Correlated Single Photon Counting (TCSPC) using a FluoTime 300 photoluminescence lifetime and steady-state spectrometer (PicoQuant). Excitation was carried out using a pulsed laser diode at 475 nm, operating at 40 MHz, with a pulse width of approximately 25 ps. The detector PMA Hybrid 50 was used. The emission was monitored at 720 nm with a bandwidth of 27 nm. The measurements were performed on devices without scattering layers and at open-circuit conditions.

3. RESULTS AND DISCUSSION

Among other assets, the electrolyte solvent must display high ionic mobility and adequate solubility of the redox species.[6,7] For that reason, the viscosity, boiling point, dielectric constant, and donor number are among the most critical physical properties in the selection of the electrolyte solvent. These properties determined the selection of the solvents tested as electrolyte solvent for M-DSSCs: ACN, MPN, PC, GBL, and NMP.

3.1. Electrochemical Characterization of Electrolytes Prepared with Different Solvents

Electrolytes prepared with the selected solvents were electrochemically characterized in symmetrical half-cells (Figure 3, Table 2). The limiting diffusion current density (j_L) and the diffusion coefficient (D) were extracted from the cyclic voltammetry (CV), while the series resistance (R_S), the charge-transfer resistance at the electrolyte/electrode interface (R_E), and the modulus of the Warburg impedance (W_S) were obtained from the electrochemical impedance spectroscopy (EIS) spectra.

The Nyquist plots of the symmetrical half-cells showed two semi-circles; the first semi-circle, at higher frequencies, corresponds to the Cu(I)/Cu(II) redox reaction at the interface between the carbon counter-electrode and the electrolyte solution, while the second semi-circle, at lower frequencies, relates to the diffusion of the redox species.[25]

The j_L is determined by the mass transport in the diffusion-limited region at high potentials,[17,26] corresponding to the plateau in the cyclic voltammogram; j_L is correlated with the diffusion coefficient (D) through eq 1:

$$j_L = \frac{2 \cdot F \cdot n \cdot D \cdot c}{\delta} \quad (1)$$

where F is the Faraday constant (F = 96 500 A s mol^{-1}), n is the number of electrons (n = 1), c is the concentration of

https://doi.org/10.1021/acsaem.6c01356
ACS Appl. Energy Mater. 2026, 9, 8868−8878

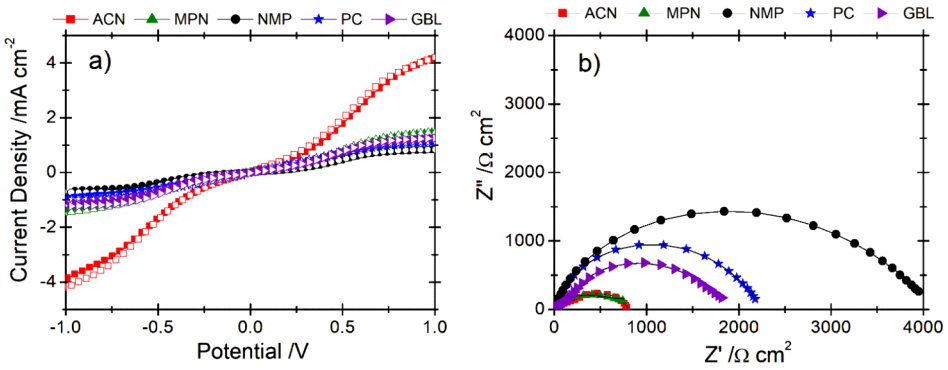

Figure 3. Cyclic voltammograms in reverse (filled symbols) and forward (empty symbols) scans (a); Nyquist plots for the EIS response of symmetrical half-cells (b). Solid lines are the fittings obtained using the electrical equivalent circuit shown in the Section.

Table 2. Electrochemical Parameters of the Electrolytes Prepared with the Different Solvents, Characterized in Symmetrical Half-Cells

electrolyte solvent	j_L/mA cm^{-2}	D/cm^2 s^{-1}	R_S/Ω cm^2	R_E/Ω cm^2	W_S/Ω cm^2
ACN	4.20	6.53×10^{-6}	1.7	3.6	286.1
MPN	1.47	2.29×10^{-6}	2.1	7.2	416.5
NMP	0.83	1.30×10^{-6}	2.0	36.0	1473.8
PC	1.10	1.71×10^{-6}	2.0	18.0	839.9
GBL	1.26	1.95×10^{-6}	2.0	25.9	636.8

diffusion limited-species in the electrolyte solution ($c = 0.04$ M for $Cu(tmby)_2^{2+}$), and δ is the distance between the two substrates, given by the thickness of the thermoplastic sealant ($\delta = 120$ μm).

Among the tested solvents, ACN-based systems exhibited the lowest R_E and W_S and the highest j_L and D, indicating the fastest charge-transfer kinetics and enhanced diffusion of the redox species.[10]

MPN presents a dielectric constant close to those of ACN. However, the higher boiling point of MPN may help slow solvent evaporation, thereby contributing to the long-term performance of DSSCs. For this reason, MPN has been widely used as an alternative to ACN for DSSCs operating indoors. Indeed, with the exception of ACN-based devices, the MPN symmetrical half cells showed the lowest R_E and W_S, and the highest j_L and D.

Among the remaining solvents (NMP, PC, GBL), NMP exhibited the highest resistances and the lowest j_L and D. NMP has a high donor number, which may benefit the solubility of salts and stabilize charges, but has the drawback of decreasing ionic diffusion through the formation of stronger and larger complexes, lowering j_L and D.[11]

A high dielectric constant facilitates the dissociation of salts and improves the ionic conductivity, while viscosity influences ionic mobility.[27] Consequently, it is essential to balance a high electric constant with a viscosity that does not compromise the ionic diffusion. Among the tested solvents, PC presents the highest dielectric constant but also the highest viscosity, contributing to a lower j_L and D than GBL, ACN and MPN, and a higher W_S.

3.2. Photovoltaic Behavior of M-DSSCs under AM1.5G Light

The photovoltaic performance of the devices loaded with the selected electrolytes was assessed using photocurrent *vs.* potential ($J-V$) measurements (Figure 4); internal resistances of the cells were determined by EIS analysis (Figure S4). The averaged PV metrics (open-circuit voltage - V_{OC}; short-circuit current - J_{SC}; fill factor - FF; power conversion efficiency - PCE) and EIS parameters (series resistance - R_S; charge transfer resistance at counter-electrode/electrolyte interface - R_{CE}; recombination resistance at TiO_2/electrolyte interface - R_K; modulus of the Warburg impedance - W_S) of three identical devices are listed in Table 3 for each solvent.

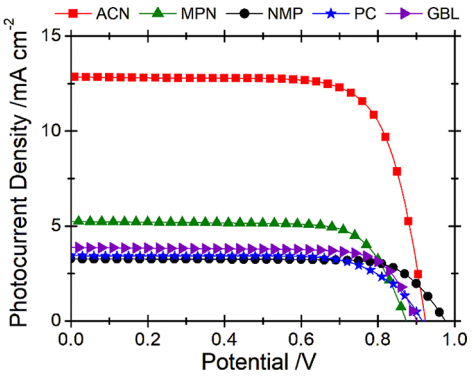

Figure 4. $J-V$ curves of M-DSSCs with different electrolyte solvents under AM1.5G.

The DSSCs loaded with ACN presented the highest J_{SC} and PCE under AM1.5G, which is supported by the highest diffusion coefficient of the ionic species, D, determined in symmetrical half-cells. Although MPN and ACN possess similar dielectric constants, MPN showed a lower D, which limits redox-species diffusion, slows the dye-regeneration kinetics, and also hinders the regeneration of oxidized Cu(II) species at the counter-electrode. As a result, devices based on MPN exhibited lower V_{OC}, J_{SC} and PCE values.

https://doi.org/10.1021/acsaem.6c01356
ACS Appl. Energy Mater. 2026, 9, 8868−8878

Table 3. PV Metrics and Parameters Extracted from the EIS Spectra of the M-DSSCs Using Different Electrolyte Solvents under AM1.5G

electrolyte solvent	V_{OC} (V)	J_{SC} (mA cm^{-2})	FF	PCE (%)	R_S (Ω cm^2)	R_{CE} (Ω cm^2)	R_K (Ω cm^2)	W_S (Ω cm^2)
ACN	0.920 ± 0.001	12.8 ± 0.1	0.745 ± 0.001	9.0 ± 0.1	12.4 ± 0.4	13.9 ± 0.9	15.4 ± 1.0	22.6 ± 0.2
MPN	0.873 ± 0.001	5.2 ± 0.1	0.738 ± 0.005	3.5 ± 0.1	15.2 ± 0.3	20.8 ± 1.0	32.0 ± 2.0	40.0 ± 2.5
NMP	0.969 ± 0.009	3.4 ± 0.2	0.728 ± 0.037	2.3 ± 0.1	14.9 ± 0.5	22.3 ± 1.2	56.0 ± 1.5	160.0 ± 4.5
PC	0.923 ± 0.005	3.2 ± 0.2	0.755 ± 0.041	2.2 ± 0.3	15.0 ± 0.4	27.2 ± 0.8	41.6 ± 1.3	80.0 ± 3.5
GBL	0.900 ± 0.001	3.7 ± 0.2	0.725 ± 0.034	2.4 ± 0.2	16.0 ± 0.3	26.4 ± 0.9	40.0 ± 1.4	56.0 ± 3.7

Cells loaded with MPN solvent displayed higher J_{SC} and PCE than counterparts loaded with NMP, PC, or GBL solvents, due to the higher D of MPN. In turn, DSSC with NMP shows the highest V_{OC}, which is attributed, among other factors, to its higher donor number.[9,10]

Additional information regarding the charge transfer in different electrolyte media was obtained using EIS (Figure S4). As expected, the ACN-based M-DSSC showed the lowest R_{CE}, R_K, and W_S, resulting in the highest energy-performing devices. DSSCs using MPN, the most used solvent to replace ACN, displayed lower R_{CE}, R_K, and W_S than the devices using NMP, PC, or GBL solvents. The devices loaded with NMP solvents presented a R_K higher than the other solvents, which was attributed to its high donor number, increasing the probability of being adsorbed at the TiO_2 surface – resulting in the highest adsorption energy,[9] thereby mitigating the recombination reaction at the TiO_2/electrolyte interface.

Among the parameters extracted from the Nyquist plots, the diffusion resistance, W_S, was the most affected by the nature of the solvent, being directly related to the diffusion coefficient of the ionic species. The lower W_S was obtained with ACN and MPN-based devices, while the highest W_S was reached with NMP-based devices, in agreement with the results obtained with the symmetrical half cells.

3.3. Photovoltaic Performance of M-DSSCs under Indoor Illumination

Under indoor illumination, MPN has been used as an electrolyte solvent in detriment of ACN.[4,5,14,20,21] MPN displays a similar donor number and dielectric constant to ACN, but lower volatility, which improves its stability. Another nitrile-based solvent, propionitrile, was tested and found to underperform compared to ACN-based devices.[14] γ-valerolactone was recently proposed as an alternative to ACN for indoor iodide-mediated DSSCs, achieving higher PCEs than the equivalent cells loaded with ACN or MPN.[22]

In the present work, the fabricated DSSCs were characterized under indoor illumination of 300, 600, and 1000 lx; the J–V curves are displayed in Figure 5, and the corresponding PV metrics are presented in Table 4.

The NMP solvent, which showed comparable PCEs to PC and GBL devices under AM1.5G (PCE = 2.3 ± 0.1%), displayed poor performance under indoor illumination (PCE = 14.4 ± 0.1%, 1000 lx). Among the proposed solvents, NMP

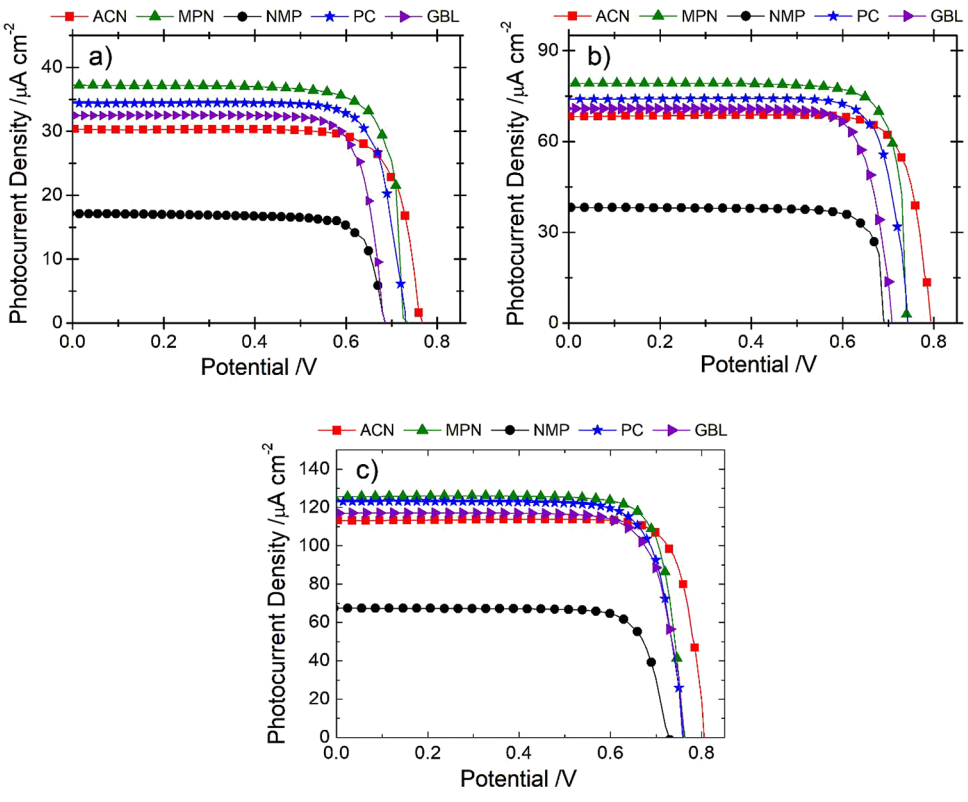

Figure 5. J–V curves of M-DSSCs with different electrolyte solvents under 300 lx (a), 600 lx (b), and 1000 lx (c).

https://doi.org/10.1021/acsaem.6c01356
ACS Appl. Energy Mater. 2026, 9, 8868−8878

Table 4. PV Metrics of the M-DSSCs Using Different Electrolyte Solvents under Different Ambient Light Intensities (300, 600, and 1000 lx)

	300 lx				600 lx				1000 lx			
electrolyte solvent	V_{OC}/V	J_{SC}/μA cm^{-2}	FF	PCE/%	V_{OC}/V	J_{SC}/μA cm^{-2}	FF	PCE/%	V_{OC}/V	J_{SC}/μA cm^{-2}	FF	PCE/%
ACN	0.775 ± 0.002	30.7 ± 0.3	0.760 ± 0.001	23.1 ± 0.3	0.795 ± 0.001	68.0 ± 0.4	0.807 ± 0.001	26.7 ± 0.2	0.804 ± 0.002	113.0 ± 0.5	0.820 ± 0.001	27.4 ± 0.2
MPN	**0.742 ± 0.002**	**37.2 ± 0.2**	**0.782 ± 0.002**	**27.6 ± 0.3**	**0.755 ± 0.002**	**76.3 ± 0.5**	**0.805 ± 0.001**	**28.4 ± 0.3**	**0.765 ± 0.002**	**125.5 ± 0.6**	**0.809 ± 0.001**	**28.5 ± 0.2**
NMP	0.685 ± 0.001	17.1 ± 0.3	0.789 ± 0.001	11.8 ± 0.2	0.697 ± 0.002	38.5 ± 0.6	0.824 ± 0.002	13.5 ± 0.3	0.735 ± 0.001	67.5 ± 0.4	0.787 ± 0.001	14.4 ± 0.1
PC	**0.735 ± 0.001**	**35.1 ± 0.7**	**0.786 ± 0.002**	**26.0 ± 0.5**	**0.745 ± 0.002**	**74.0 ± 0.4**	**0.804 ± 0.002**	**27.1 ± 0.3**	**0.755 ± 0.002**	**123.1 ± 0.8**	**0.792 ± 0.001**	**27.1 ± 0.2**
GBL	0.680 ± 0.001	32.5 ± 0.5	0.805 ± 0.001	22.7 ± 0.3	0.705 ± 0.001	70.9 ± 0.5	0.798 ± 0.001	24.4 ± 0.2	0.764 ± 0.002	116.5 ± 0.6	0.784 ± 0.002	25.7 ± 0.2

has the highest dye desorption from the TiO_2 layer (Figure S5). Under AM1.5G, this effect was not apparent due to the overall low photovoltaic performance. In contrast, under indoor illumination conditions, the impact of dye desorption was more pronounced, resulting in lower J_{SC} in comparison with the other solvents.

The performance of cells fabricated with other solvents (ACN, MPN, PC, and GLB) was quite surprising as PCEs exceeded 25% under 1000 lx. The DSSCs loaded with ACN showed the best PCEs of 9.0 ± 0.1% under AM.1.5G, and displayed a PCE of 27.4 ± 0.2% under 1000 lx. Thus, the MPN-based cells (28.5 ± 0.2%) outperformed the ACN-DSSCs, and exhibited comparable PCE with PC-DSSCs (27.1 ± 0.2%). Unpredictably, the MPN and PC-based DSSCs exhibited high PCEs (>25%) even under lower light conditions (300 and 600 lx). These PV performance result from a smaller decrease in V_{OC} and a higher FF under lower light.

EIS spectra were recorded under 300, 600, and 1000 lx to obtain additional information regarding charge transfer when different electrolyte solvents are used (Figure S6, Table S2). Under indoor illumination, the EIS spectra of DSSCs revealed two semi-circles, associated with the charge transfer resistance at the counter-electrode/electrolyte and at the mesoporous TiO_2/electrolyte interfaces, at higher and lower frequencies, respectively. Sánchez-Fernández et al.[28] reported that under low-light conditions, the dye regeneration is less dependent on the ionic diffusion in the electrolyte medium. The second semi-circle enlarges as the light intensity decreases, indicating that the recombination kinetics decrease.[28,29] From the EIS spectra, the internal resistances (R_S, R_{CE}, R_K) for the prepared cells were extracted; the electron diffusion length (L_n), the recombination lifetime (τ_R), and the electron collection efficiency (η_{col}) were determined using the following equations:[10,30,31]

$$L_n = d \times \sqrt{\frac{R_K}{R_{CE}}} \tag{2}$$

$$\eta_{col} = 1 - \frac{R_{CE}}{R_K} \tag{3}$$

$$\tau_R = C_\mu \times R_K \cong \frac{1}{2\pi f_{max}} \tag{4}$$

where d is the thickness of the TiO_2 layer, C_μ is the chemical capacitance of the mesoporous TiO_2 layer, and f_{max} corresponds to the maximum frequency of a phase shift peak in the Bode plot (Figure S7). All these parameters extracted from EIS data were plotted as a function of the incident light intensity (Figure 6).

Regardless of the light intensity, the R_S presented slight fluctuations among all devices, while the R_{CE} and R_K increased as the light intensity decreased. Sánchez-Fernández et al.[27] reported that the charge transport in iodide-mediated DSSCs under indoor illumination decelerated more rapidly than recombination when the irradiance decreased using EIS data. This is noticeable when the increase in R_{CE} is more pronounced than the increase in R_K; this is detrimental to the PV performance when L_n decreases. These authors used this tendency to support the fact that DSSCs with a PCE of 8% under AM1.5G underperformed under ambient light, achieving

https://doi.org/10.1021/acsaem.6c01356
ACS Appl. Energy Mater. 2026, 9, 8868−8878

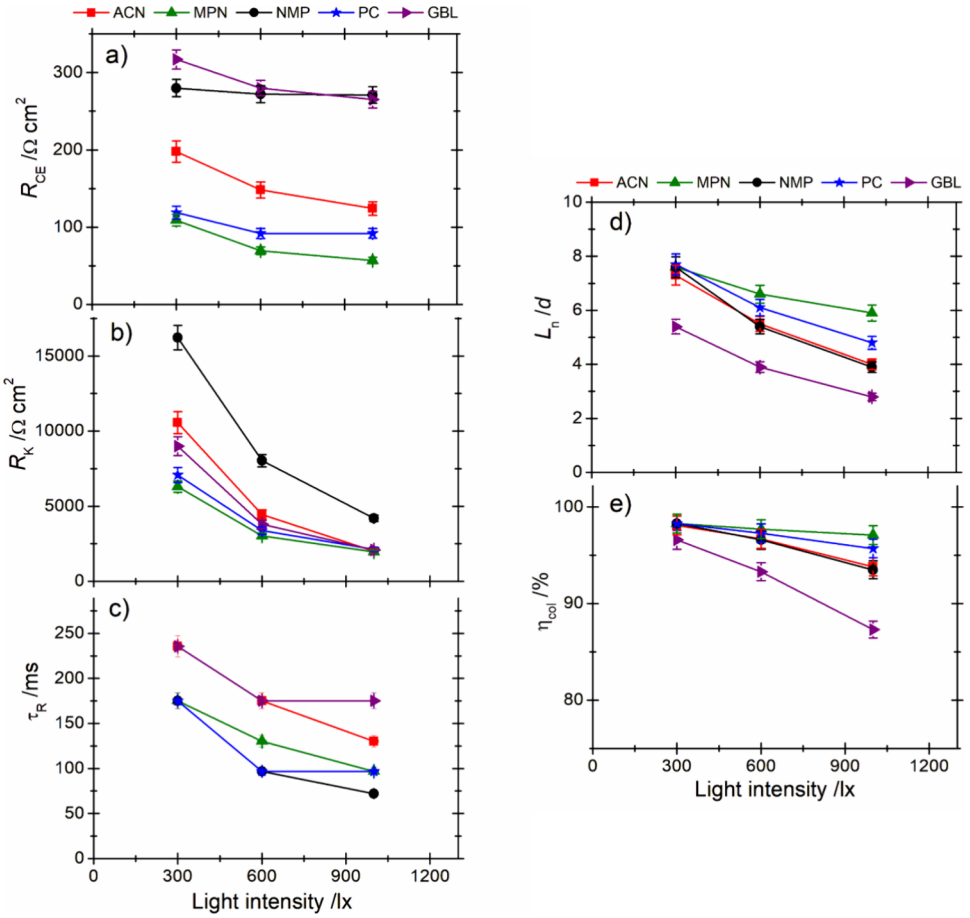

Figure 6. R_{CE} (a), R_K (b), τ_R (c), L_n/d (d), and e η_{col} (e) in function of the light intensity (300−1000 lx).

PCEs of 15%. An opposite tendency was observed in this work when copper-mediated DSSCs using different electrolyte solvents were studied. Independent of the solvent, the recombination reactions decelerated more quickly than the charge transport reactions as the illumination intensity decreased, showing a higher increase in R_K compared to R_{CE}. This hypothesis is supported by higher τ_R, L_n, and η_{col} under lower indoor illumination[26] (Figure 6c−e, Table S2). Sánchez-Fernández et al.[28] claimed that $L_n/d < 3$ may compromise electron collection; in iodide-mediated DSSCs, the same authors reported $L_n/d < 2$ under low ambient light intensity, which is a strong indication of electron collection losses, associated with fast recombination and slow transport reactions.[27] The copper-mediated DSSCs prepared in this work displayed an opposite correlation between the reaction's kinetics and the illuminance, since the L_n/d increases when the light intensity decreases (Figure 6e). It should be emphasized that the only device showing $L_n/d < 3$ is the GBL-based M-DSSC under 1000 lx. This suggests that copper-mediated DSSCs can retain a high PCE even under weak illumination of 200−300 lx.

For all tested light intensities, the DSSCs using MPN and PC electrolyte solvents displayed the lowest R_K and $R_{CE,}$ and the highest L_n/d and η_{col}. In fact, these devices proved to be the most efficient under indoor illumination, outperforming ACN-based DSSCs; PCEs >25% were obtained across the entire range of tested light intensities, from 300 to 1000 lx.

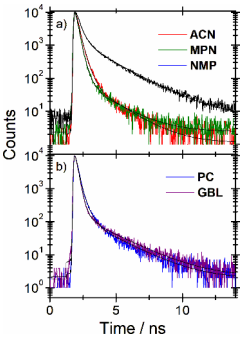

Figure 7. Photoluminescence decay for photoanodes in contact with electrolytes prepared with ACN, MPN, NMP (a), PC and GBL (b) solvents. Black lines stand for fitting.

Time-Correlated Single Photon Counting (TCSPC) experiments were performed to evaluate the lifetimes of the photoexcited states of the dye in electrolytes prepared with the different solvents (Figure 7).

The photoluminescence decay of TiO_2/Y123 photoanodes is well fitted with a bi-exponential model. The component with the longer relaxation time, τ_1, in the range of 1.7−2.2 ns, and lower relative intensity, I_{Rel1}, is due to radiative relaxation of the dye. The fast component, with a lifetime τ_2 in the range of 0.22−0.33 ns and dominant relative intensities I_{Rel2}, is

https://doi.org/10.1021/acsaem.6c01356
ACS Appl. Energy Mater. 2026, 9, 8868−8878

Table 5. Results from the Fitting of the Photoluminescence Decay of the Devices[a]

solvent	τ_1/ns	I_{Rel1}	τ_2/ns	I_{Rel2}	τ_m/ns
ACN	1.659 ± 0.097	10 ± 0.5	0.284 ± 0.006	90.1 ± 0.5	0.422
MPN	1.796 ± 0.085	12.4 ± 0.7	0.241 ± 0.003	87.7 ± 0.7	0.434
NMP	1.995 ± 0.029	48.6 ± 0.4	0.332 ± 0.015	51.5 ± 0.4	1.139
PC	2.06 ± 0.11	20.9 ± 0.9	0.318 ± 0.022	79.2 ± 0.9	0.682
GBL	2.182 ± 0.053	28.8 ± 0.6	0.221 ± 0.012	71.3 ± 0.6	0.785

[a]The lifetime (τ_i) and relative intensity (I_{Reli}) of the two contributions are reported.

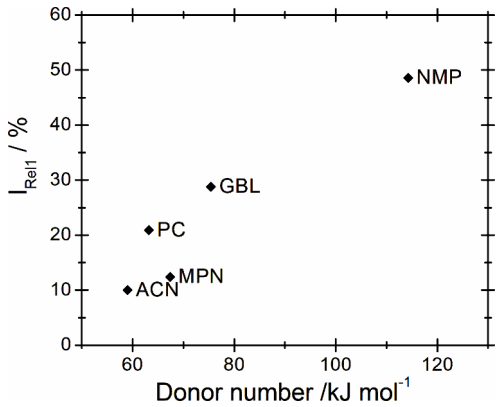

Figure 8. Relative intensity of slow radiative relaxation decay I_{Rel1} vs donor number (DN) of the solvent.

affected by electron injection from the excited dye into TiO_2 layer.[32,33] Table 5 shows the fitting results using a two-exponential function and intensity-weighted mean lifetimes $\tau_m = (\tau_1 \cdot I_{Rel1} + \tau_2 \cdot I_{Rel2})/(I_{Rel1} + I_{Rel2})$ for each solvent.

The obtained TRPL data correlate well with the device performance at low light intensities (Table 4). An illumination level of 300 lx represents typical indoor operating conditions for DSSCs and provides the clearest differentiation among the photovoltaic performance metrics; lower incident light allows clearer observation of injection/recombination dynamics, which are often masked at higher irradiations where charge transport and saturation effects start to dominate.

A clear trend is observed between the solvent donor number (DN) (Table 1) and the fraction of the slow and fast components in the TRPL decay (Figure 8).

A higher donor number results in larger I_{Rel1} values, and consequently in a lower I_{Rel2}, and longer mean lifetimes τ_m (Table 5). Low donor number solvents, such as ACN and MPN, (DN ca. 14−16), exhibit low I_{Rel1} (10−12%) and short τ_m (~0.43 ns), while high donor number NMP (DN 27.3) shows an I_{Rel1} of ca. 50% and the longest τ_m (1.12 ns). This correlation indicates that stronger Lewis basicity favors the coordination of solvent to the TiO_2/dye interface; the electron injection is decelerated, and the emissive recombination states are increased, which in turn results in lower values of V_{OC}, J_{SC}, and PCE under 300 lx (Table 4).

In more detail, larger values of I_{Rel2} and shorter values of τ_2 are associated with a higher rate of electron injection from dye to titania and shorter time for radiative loss. Considering that the obtained values of τ_2 are in the range of 0.2−0.3 ns, the contribution of I_{Rel2} becomes decisive for the J_{SC} (Figure 9a).

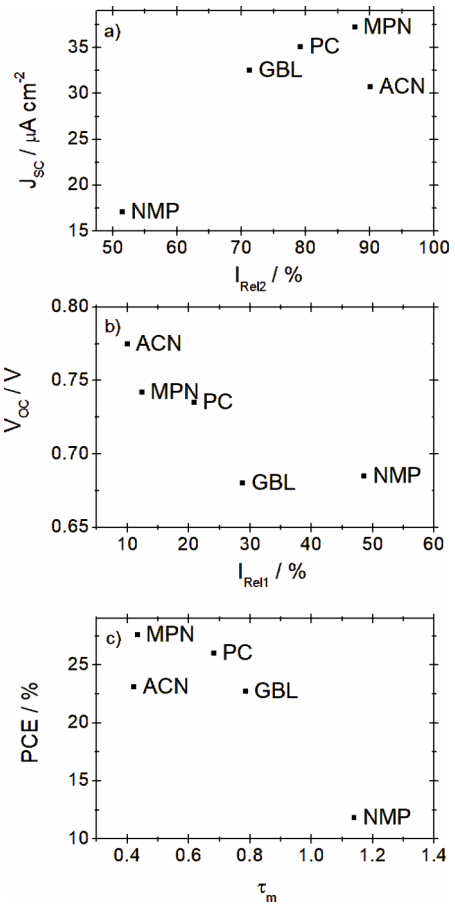

Figure 9. Correlation between TRPL-derived parameters and photovoltaic performance of DSSCs under 300 lx: J_{SC} vs I_{Rel2} (a); V_{OC} vs I_{Rel1} (b); and overall PCE vs τ_m (c).

Conversely, V_{OC} decreases as I_{Rel1} increases (Figure 9b), which indicates that a larger slow population corresponds to stronger recombination and V_{OC} loss. Overall, a clear inverse correlation is observed between the average lifetime (τ_m) and PCE – Figure 9c; shorter recombination times signify more efficient charge separation and faster electron injection into TiO_2.

The TRPL data indicate that charge injection and recombination kinetics in DSSCs are strongly influenced by the electrolyte solvent, with the donor number playing a key role in governing the balance between fast and slow excited-state decay pathways. This donor number-dependent modulation of excited state dynamics appears to play a role, among other factors, in determining device PCE under weak indoor light.

3.4. Stability of Copper-Mediated M-DSSCs under Indoor Light

M-DSSCs loaded with MPN and PC solvents displayed PCEs >25% under light intensities ranging from 300 to 1000 lx, whereas the devices loaded with ACN and GBL showed a higher PCE drop at low light intensities. Therefore, MPN and PC solvents emerge as the best for indoor applications, where the light intensity typically does not exceed 300 lx. Still, the stability of these devices must be evaluated to assess their potential for becoming commercial. For this reason, the PV performance of copper-mediated DSSCs loaded with the selected electrolyte solvents (ACN, MPN, PC, GBL) was followed for 1000 h

https://doi.org/10.1021/acsaem.6c01356
ACS Appl. Energy Mater. 2026, 9, 8868−8878

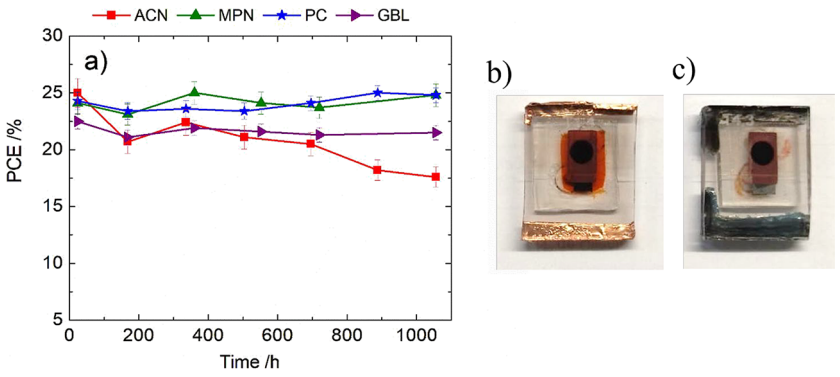

Figure 10. PCE vs time of M-DSSCs under 1000 lx illumination (a); photograph of PC-DSSC (b) and ACN-DSSC (c) at the end of the experiment.

under 1000 lx light soaking; all the devices presented an initial PCE of 22.5−25.0%, and for each condition, 5 identical cells were prepared. NMP-based devices were not considered, as they exhibited significantly poorer performance compared to the other electrolyte solvents. During the entire experiment, the devices were kept at ca. 25 °C and ca. 70% RH, and operated at their maximum power point using an adjustable external resistance. Figure 10 plots the PCE as a function of time for the tested copper-mediated DSSCs; the evaluation of the remaining PV metrics as a function of time is plotted in Figure S8.

During the experiment, the ACN-based DSSCs exhibited electrolyte leakage through the sealing perimeter (Figure 10c), most likely due to the high volatility of acetonitrile. As a consequence, these devices showed a pronounced deterioration in PCE, with a decrease of ca. 30% after 1000 h of continuous indoor illumination. Electrolyte leakage was not observed in the DSSCs loaded with the remaining solvents, which explains why these devices exhibited greater stability and smaller PCE variations over the same period, namely −4% for GBL, +2% for PC, and +3% for MPN.

The DSSC devices loaded with GBL exhibited PCEs > 20% under indoor illumination and a steady history of PV metrics. However, GBL raises concerns related to its toxicity.[34,35] The highest-energy-performing and stable devices were fabricated using MPN or PC as electrolyte solvent. Furthermore, PC is often considered a "green" solvent, due to its biodegradability and low toxicity,[36] whereas MPN may cause skin and respiratory system irritations and could release toxic gases when in contact with acids.[37,38] This work introduces for the first time PC as a non-toxic electrolyte solvent for highly efficient copper-mediated indoor DSSCs; these devices are able to retain stable and high PCEs (26.0 ± 0.5%), even under light conditions as low as 300 lx.

4. CONCLUSIONS

Copper-mediated monolithic dye-sensitized solar cells (M-DSSCs) employing different electrolyte solvents (ACN, MPN, NMP, PC, and GBL) were systematically fabricated and evaluated under simulated AM1.5G and indoor illumination conditions (300, 600, and 1000 lx). Under AM1.5G irradiation, the devices using acetonitrile (ACN) displayed the highest photovoltaic performance. In contrast, under low-intensity indoor illumination, ACN-based devices were outperformed by DSSCs employing 3-methoxypropionitrile (MPN) and propylene carbonate (PC). These devices exhibited the lowest recombination resistance (R_K) and charge-transfer resistance (R_{CE}), together with the highest electron collection efficiency (η_{col}) and normalized diffusion length (L_n/d). As a result, MPN- and PC-based DSSCs achieved power conversion efficiencies exceeding 25% even under weak illumination of 300 lx.

Importantly, the lower volatility of MPN and PC solvents (in comparison with ACN) slowed the electrolyte evaporation, enabling stable device operation for over 1000 h under continuous indoor illumination at 1000 lx. Conversely, ACN-based devices suffered from solvent leakage and exhibited a significant performance degradation of ca. 30%.

Time-resolved photoluminescence (TRPL) analyses revealed that the electrolyte solvent donor number (DN) plays a crucial role in governing interfacial charge-transfer dynamics. Low-DN solvents (ACN and MPN) favored faster electron injection and shorter mean lifetimes (τ_m), consistent with enhanced short-circuit current density and higher indoor efficiencies. On the other hand, high-DN solvents such as NMP promoted slower decay pathways and longer τ_m, indicative of increased recombination losses. This DN-dependent photophysical behavior provides a mechanistic framework linking solvent properties, interfacial kinetics, and device performance under artificial light.

Overall, PC and MPN emerged as the most effective electrolyte solvents for indoor DSSCs, combining high efficiency with excellent operational stability. Among them, PC offers additional advantages in terms of lower toxicity and improved environmental compatibility. This work therefore identifies propylene carbonate as a safe and sustainable alternative to conventional nitrile-based solvents, capable of delivering high efficiency, robust long-term stability, and favorable excited-state and charge-transfer dynamics for indoor photovoltaic applications.

■ ASSOCIATED CONTENT

Supporting Information

The Supporting Information is available free of charge at https://pubs.acs.org/doi/10.1021/acsaem.6c01356.

Chemical structure of dyes and copper complexes; emission spectra of LED lamp; parameters extracted from $J-V$ curves of devices at 1000 lx but different working distances between LED lamp and M-DSSCs; photograph of indoor characterization set-up; Nyquist plots of M-DSSC with different solvents under AM1.5G; transmittance of TiO_2+dye photoanodes; Nyquist and Bode

https://doi.org/10.1021/acsaem.6c01356
ACS Appl. Energy Mater. 2026, 9, 8868−8878

plots of M-DSSCs with different solvents under indoor light; and history of PV metrics under 1000 lx (DOCX)

AUTHOR INFORMATION

Corresponding Author

Fátima Santos – *LEPABE – Laboratory for Process Engineering, Environment, Biotechnology and Energy, ALiCE – Associate Laboratory in Chemical Engineering, Faculty of Engineering, University of Porto, Rua Dr. Roberto Frias, 4200-465 Porto, Portugal*; orcid.org/0000-0002-9029-4107; Email: feosantos@fe.up.pt

Authors

Dzmitry Ivanou – *LEPABE – Laboratory for Process Engineering, Environment, Biotechnology and Energy, ALiCE – Associate Laboratory in Chemical Engineering, Faculty of Engineering, University of Porto, Rua Dr. Roberto Frias, 4200-465 Porto, Portugal*; orcid.org/0000-0002-5313-4016

Adélio Mendes – *LEPABE – Laboratory for Process Engineering, Environment, Biotechnology and Energy, ALiCE – Associate Laboratory in Chemical Engineering, Faculty of Engineering, University of Porto, Rua Dr. Roberto Frias, 4200-465 Porto, Portugal*; orcid.org/0000-0003-2472-3265

Complete contact information is available at: https://pubs.acs.org/doi/10.1021/acsaem.6c01356

Author Contributions

F.S. – research idea; device preparation and characterization; literature rev., draft of the article; D.I. – scientific discussion; TCSPC experiments and interpretation; A.M. – conceptualization; funding; scientific discussion. All the authors contributed to the manuscript preparation.

Notes

The authors declare no competing financial interest.

ACKNOWLEDGMENTS

F.S. acknowledges the FCT for her research grant reference 2023.07366.CEECIND/CP2834/CT0012 (DOI: 10.54499/2023.07366.CEECIND/CP2834/CT0012). D.I. acknowledges the project CEECINST/00010/2021/CP1770/CT0002. The research leading to these results also received funding from: (i) Agenda "AET – Alliance for Energy Transition", nr. C644914747-00000023, investment project nr. 56, financed by the Recovery and Resilience Plan (PRR) and by European Union - NextGeneration EU; (ii) Project SMART&GREEN, NORTE2030-FEDER-02696100, financed by CCDR NORTE; (iii) Project DreamPEC, nr. 15308 operation code at the Funds Platform COMPETE2030-FEDER-00898000, financed by COMPETE 2030, Portugal 2030, European Union, and FCT; (iv) Project "PVBoost – Indoor photovoltaics for powering IoT electronics", with nr. 18334 and operation code NORTE2030-FEDER-01463100, co-financed by the European Union through the NORTE 2030 Regional Programme, of Portugal 2030; and (v) national funds through FCT/MECI: LEPABE, UID/00511/2025 (DOI: 10.54499/UID/00511/2025) and UID/PRR/00511/2025 (DOI: 10.54499/UID/PRR/00511/2025) and ALiCE, LA/P/0045/2020 (DOI: 10.54499/LA/P/0045/2020). The authors are thankful to Carlos Gabriel Bernardo (ORCID: 0000-0001-7392-4915) for contribution in PVBoost draft preparation.

REFERENCES

(1) Muñoz-García, A. B.; Benesperi, I.; Boschloo, G.; Concepcion, J. J.; Delcamp, J. H.; Gibson, E. A.; Meyer, G. J.; Pavone, M.; Petterson, H.; Hagfeldt, A.; Freitag, M. Dye-sensitized solar cells strike back. *Chem. Soc. Rev.* **2021**, *50*, 12450–12550.

(2) Müller, D.; Jiang, E.; Rivas-Lazaro, P.; Baretzky, C.; Loukeris, G.; Bogati, S.; Paetel, S.; Irvine, S. J. C.; Oklobia, O.; Jones, S.; Lamb, D.; Richter, A.; Siefer, G.; Lackner, D.; Helmers, H.; Teixeira, C.; Forgács, D.; Freitag, M.; Bradford, D.; Shen, Z.; Zimmermann, B.; Würfel, U. Indoor Photovoltaics for the Internet-of-Things – A Comparison of State-of-the-Art Devices from Different Photovoltaic Technologies. *ACS Appl. Energy Mater.* **2023**, *6*(20), 10404–10414.

(3) Jebin, P. R.; George, A. S.; Mishra, R. K.; John, J.; Soman, S. Enhanced indoor photovoltaic efficiency of 40% in dye-sensitized solar cells using cocktail starburst triphenylamine dyes and dual-species copper electrolyte. *J. Mater. Chem. A* **2024**, *12*, 32721–32734.

(4) Michaels, H.; Rinderle, M.; Benesperi, I.; Freitag, R.; Gagliardi, A.; Freitag, M. Emerging indoor photovoltaics for self-powered and self-aware IoT towards sustainable energy management. *Chem. Sci.* **2023**, *14*, 5350.

(5) Ren, Y.; Zhang, D.; Suo, J.; Cao, Y.; Eickemeyer, F.T.; Vlachopoulos, N.; Zakeeruddin, S. M.; Hagfeldt, A.; Grätzel, M. Hydroxamic acid preadsorption raises efficiency of cosensitized solar cells. *Nature* **2022**, *613*, 60–65.

(6) Masud; Kim, H. K. Redox Shuttle-Based Electrolytes for Dye-Sensitized Solar Cells: Comprehensive Guidance, Recent Progress, and Future Perspective *ACS Omega* **2023**, *8*, 6139–6163.

(7) Wu, J.; Lan, Z.; Lin, J.; Huang, M.; Huang, Y.; Fan, L.; Luo, G. Eletrolytes in Dye-Sensitized Solar Cells. *Chem. Rev.* **2015**, *115*, 3, 2136–2173.

(8) Rosa, E. S.; Septina, W.; Shobih; Megananda, P. C.; Hardian, A.; Nursam, N. M. Improved efficiency and stability of dye-sensitized solar cells by using iodide-based electrolyte with high viscosity solvent. *Mater. Lett.* **2024**, *358*, 135847.

(9) Mohanty, S. P.; Bhargava, P. Impact of Electrolytes Based on Different Solvents on the Long Term Stability of Dye Sensitized Solar Cells. *Electrochim. Acta* **2015**, *168*, 111–115.

(10) Tao, R.; Timuda, G. E.; Waki, K. Electrochemical analysis of dye sensitized solar cell employing indoline-based and ruthenium-based dye combined with volatile and low-volatility solution-based electrolyte. *J. Mater. Sci.: Mater. Electron.* **2018**, *29*, 19245–19255.

(11) Wu, J.; Lan, Z.; Lin, J.; Huang, M.; Li, P. Effect of solvents in liquid electrolyte on the photovoltaic performance of dye-sensitized solar cells. *J. Power Sources* **2007**, *173*, 585–591.

(12) Gondane, V.; Bhargava, P. Acetylacetone: a promising electrolyte solvent for dye sensitized solar cells. *RSC Adv.*, **2016**, *6*, 37167.

(13) Shi, D.; Pootrakulchote, N.; Li, R.; Guo, J.; Wang, Y.; Zakeeruddin, S. M.; Gratzel, M.; Wang, P. New Efficiency Records for Stable Dye-Sensitized Solar Cells with Low-Volatility and Ionic Liquid Electrolytes. *J. Phys. Chem. C* **2008**, *112*, 17046–17050.

(14) Freitag, M.; Teuscher, J.; Saygili, Y.; Zhang, X.; Giordano, F.; Liska, P.; Hua, J.; Zakeeruddin, S. M.; Moser, J.-E.; Grätzel, M.; Hagfeldt, A. Dye-sensitized solar cells for efficient power generation under ambient lighting. *Nat. Photonics* **2017**, *11*, 372–378.

(15) Cao, Y.; Liu, Y.; Zakeeruddin, S. M.; Hagfeldt, A.; Grätzel, M. Direct Contact of Selective Charge Extraction Layers Enables High-Efficiency Molecular Photovoltaics. *Joule* **2018**, *2*, 1108–1117.

(16) Zhang, D.; Stojanovic, M.; Ren, Y.; Cao, Y.; Eickemeyer, F.T.; Socie, E.; Vlachopoulos, N.; Moser, J.-E.; Zakeeruddin, S. M.; Hagfeldt, A.; Grätzel, M. A molecular photosensitizer achieves a VOC of 1.24 V enabling highly efficient and stable dye-sensitized solar cells with copper(II/I)-based electrolyte. *Nat. Commun.* **2021**, *12*, 1777.

(17) Santos, F.; Ivanou, D.; Mendes, A. Solid-State Monolithic Dye-Sensitized Solar Cell Exceeding 10% Efficiency Using a

Copper-Complex Hole Transport Material and a Carbon Counter-Electrode. *Sol. RRL* **2023**, *8*, 2300574.
(18) Li, L.; Zhao, L.; Jiang, X.; Yu, Z.; Liu, J.; Rui, H.; Shen, J.; Sharmoukh, W.; Allam, N. K.; Sun, L. Efficient dye-sensitized solar cells based on bioinspired copper redox mediators by tailoring counterions. *J. Mater. Chem. A* **2022**, *10*, 4131.
(19) Masud; Zhou, H.; Kim, H. K. Effective redox shuttles for polymer gel electrolytes-based quasi-solid-state dye-sensitized solar cells in outdoor and indoor applications: Comprehensive comparison and guidelines. *Mater. Today Energy* **2023**, *34*, 101299.
(20) Ursu, D.; Casut, C.; Albulescu, D.; Vajda, M.; Mosoarca, C.; Miclau, M. Enhanced Indoor Conversion Efficiency of Dye-Sensitized Solar Cells by Optimizing Ball-Milling Process of TiO_2 Paste. *Coatings* **2024**, *14*(3), 283.
(21) Venkatesan, S.; Lin, W.-H.; Teng, H.; Lee, Y.-L. High-Efficiency Bifacial Dye-Sensitized Solar Cells for Application under Indoor Light Conditions. *ACS Appl. Mater. Interfaces* **2019**, *11*(45), 42780–47789.
(22) Speranza, R., Amenta, S., Zaccagnini, P., Pirri, C. F., Lamberti, A. Harnessing γ-Valerolactone: Green and Low-Toxic Solvent for Enhanced Dye-Sensitized Solar Cells Performance Under Indoor Lighting. *Adv. Energy Sustainability Res.* **2025**, *6*, 2400370.
(23) Khampa, W., Le, L., Passatorntaschakorn, W., Loftus, J., Jailani, J. M., Giron, F. S., Wongratanaphisan, D., Patel, C., Pecunia, V. A universal design and benchmarking framework for indoor photovoltaics. *Newton* **2026**, 100437.
(24) Jailani, J. M., Luu, A., Salvosa, E., Clegg, C., Kamalon, V.P., Nasrollahi, B. Valitova, I., Meier, S. B., Shore, A. M., Hamadani, B. H., Pecunia, V. Accurate performance characterization, reporting, and benchmarking for indoor photovoltaics. *Joule* **2025**, *9*(10), 102126.
(25) Bisquert, J. Theory of the Impedance of Electron Diffusion and Recombination in a Thin Layer. *Phys. Chem. B* **2002**, *106* (2), 325−333.
(26) Michaels, H., Benesperi, I., Edvinsson, T., Muñoz-Garcia, A. B., Pavone, M., Boschloo, G., Freitag, M. Copper Complexes with Tetradentate Ligands for Enhanced Charge Transport in Dye-Sensitized Solar Cells. *Inorganics* **2018**, *6*(2), 53.
(27) Moia, D., Abe, M., Wagner, P., Saguchi, H., Koumura, N., Nelson, J., Barnes, P. R. F., Mori, S. The Effect of the Dielectric Environment on Electron Transfer Reactions at the Interfaces of Molecular Sensitized Semiconductors in Electrolytes. *J. Phys. Chem. C* **2020**, *124*, 13, 6979–6992.
(28) Sánchez-Fernández, P.; Aranda, C. A.; Escalante, R.; Riquelme, A. J.; Demadrille, R.; Pistor, P.; Oskam, G.; Anta, J. A. Competition between Transport and Recombination in Dye Solar Cells at Low Light Intensity. *Sol. RRL* **2024**, *8*, 2400149.
(29) Sánchez-Fernández, P.; Mwalukuku, V.; Miró-Llorente, M.; Escalante, R.; Vifal-Fuentes, P.; Guc, M.; Pistor, P.; Oskam, G.; Aranda, C. A.; Anta, J. A. Impact of Transparent Conducting Oxide on the Performance of Dye-Sensitised Solar Cells for Indoor Applications. *Sol. RRL* **2025**, *9*, 2500077.
(30) Castillo-Seoane, J.; Contreras-Bernal, L.; Riquelme, A. J., Fauvel, S.; Kervella, Y.; Gil-Rostra, J.; Lozano, G.; Barranco, A.; Demadrille, R.; Sánchez-Valencia, J. R.; Borrás, A. Multidimensional nanoarchitectures for improved indoor light harvesting in dye-sensitized solar cells. *Mater. Today Energy* **2025**, *49*, 101851.
(31) Rajesh, M. N., George, A. S., Moolakkil, A., Unni, K. N. N., Prasanthkumar, S., Soman, S., Giribabu, L. Impact of ethynyl linkage on indoor photovoltaic performance of triphenylimidazole-phenothiazine dyes with dual-species copper electrolyte. *Sol. Energy* **2025**, *288*, 113264.
(32) Rodrigues, D.F.S.L., Martins, J., Sauvage, F., Abreu, C.M.R., Coelho, J. F. J., Serra, A. C., Ivanou, D., Mendes, A. Suppression of back electron recombination on the photoanode-electrolyte interface with poly(4-vinylbenzoic acid) and poly(4-vinylpyridine) co-adsorbents for stable and efficient dye-sensitized solar cells. *Surf. Interfaces* **2024**, *44*, 103627.
(33) Rodrigues, D. F. S. L., Abreu, C. M. R., Sauvage, F., Coelho, J. F. J., Serra, A. C., Ivanou, D., Mendes, A. Improved Interfacial Electron Dynamics with Block Poly(4-vinylpyridine)–Poly(styrene) Polymers for Efficient and Long-Lasting Dye-Sensitized Solar Cells. *ACS Appl. Polym. Mater.* **2024**, *6*, 15, 8939–8949.
(34) Kim, J.-H., Kim, D.-H., So, J.-H., Koo, H.-J. Toward Eco-Friendly Dye-Sensitized Solar Cells (DSSCs): Natural Dyes and Aqueous Electrolytes. *Energies* **2022**, *15*, 219.
(35) Han, J., Kim, R. H., Huang, S., Kim, J., Yun, J. S. Green Solution Processing of Halide Perovskite Solar Cells: Status and Future Directions. *Sol. RRL* **2024**, *8*, 2400262.
(36) Prudlik, A., Matei, A., Scherkus, A., Bardagi, J. I., Beil, S. B., Francke, R. On the use of propylene carbonate and dimethyl carbonate as green solvents in organic electrosynthesis. *Green Chem.* **2025**, *27*, 4280.
(37) Vaghasiya, J. V., Nandakumar, D. K., Yaoxin, Z., Tan, S. C. Low toxicity environmentally friendly single component aqueous organic ionic conductors for high efficiency photoelectrochemical solar cells. *J. Mater. Chem. A*, **2018**, *6*, 1009.
(38) Anitha, A. E., Dotter, M. A Review on Liquid Electrolyte Stability Issues for Commercialization of Dye-Sensitized Solar Cells (DSSC). *Energies* **2023**, *16*, 5129.

https://doi.org/10.1021/acsaem.6c01356
ACS Appl. Energy Mater. 2026, 9, 8868−8878